AIAA 2013-2153

Prediction of broadband fan exit guide vane response

Sheryl M. Grace * and Gilbert Forsyth †
Boston University, Boston, MA 02215

The ability to predict the broadband fan exit guide vane response to interaction with wake turbulence using a low-order method is investigated. The RSI method is used to simulate the response of the low-count vanes in the Source Diagnostic Test. The predicted pressure spectrum is compared to that measured experimentally. The predicted spectrum of the broadband vane response at all points on the vane is similar to the final acoustic spectrum, both measured and predicted, that has been presented previously in the literature. However, this means that the simulated results do not capture spectral features above 20 kHz that are present in the experimental data. The physical source of the additional spectral features must still be identified. The simulated results match the data under 20 kHz fairly well near the midspan, but underpredict the levels for frequencies below 4 kHz at positions near the hub and the tip.

I. Introduction

Many hybrid computational methods currently used to predict the broadband noise associated with the fan stage of a turbofan engine rely on a two step process. First the response of the fan exit guide vane (FEGV) is computed and then the broadband sound is calculated.[1–4] Comparisons of the final duct acoustic power predicted by these various methods have been compared against each other and against experimental findings in the past.[5] It has been shown that different modeling assumptions lead to slightly different predictions. In some cases the source of the difference is known. However, in some cases, so many modeling differences exist, it is hard to determine which are responsible for the final effects. The long term goal of this work is to determine if examination of the intermediate calculation of the vane response can help pinpoint the effects of some of the modeling assumptions.

In this paper, results from the simulation of the broadband response of a fan exit guide vane to the ingested turbulence via the RSI method[1,4] will be compared to measurements. The experimental data utilized here are taken from the Source Diagnostic Test (SDT) database. The SDT used a 22" scaled fan-rig with 22 rotor blades and different vane configurations. Vane surface pressure measurements were obtained for the low-count and low-noise vane configurations. A NASA technical report[5] describes the experiment and the data obtained. The simulations described in this paper model the low-count vane configuration.

A brief description of the RSI method is given in Section II. More details regarding the experimental data are provided in Section III. Section IV gives the comparisons between the predicted low-count vane response and the experimental data at the approach wheel speed condition.

*Assoc. Prof., Dept. of Mech. Eng., Associate Fellow, AIAA
†Graduate student, Dept. of Mech. Eng., student member

II. RSI Method

The RSI method for predicting the broadband noise produced by interaction between rotor wakes and exit guide vanes is based on a two-dimensional semianalytical solution for flat-plate cascade response to flow disturbances.[6] The wake turbulence is assumed to be convected by the mean wake flow and it is viewed as a combination of Fourier components. Each component can be modeled as a three-dimensional gust disturbance of a specified frequency and wave number. The amplitude of each gust is specified by the turbulence spectrum. Thus a spectrum model is incorporated into the method and will be discussed shortly. A strip theory is used to build the response of the entire vane to the turbulence. Once the unsteady surface pressure is calculated, it can be used to compute the acoustics downstream of the vane via the Green's function for a cylindrical annulus. Appendix A describes the method for modeling the turbulence in the wake. It is noted that the original RSI formulation included the variation of the turbulence intensity across a rotor wake passage. It was later shown that the final results for the exhaust duct broadband noise varied only slightly at high frequency when one used the average passage value of the turbulence intensity. Thus the results reported in this paper only model the average passage value at each radial location, and this is reflected in the formulation presented in the Appendix.

The correlation of the unsteady stator loading, $\langle\, \Delta\tilde{p}_j(r_1, z_1, \omega)\, \Delta\tilde{p}_l^*(r_2, z_2, \nu)\,\rangle$, can be computed given the upwash correlation, $\langle\tilde{w}\tilde{w}^*\rangle$, presented in the Appendix in Eq. (15). This may be done via the following formula.

$$\langle\, \Delta\tilde{p}_j(r_1, z_1, \omega)\, \Delta\tilde{p}_l^*(r_2, z_2, \nu)\,\rangle = \frac{(\rho_o U_r)^2}{(2\pi)^6} \int_{-\infty}^{\infty}\int_{-\infty}^{\infty}\int_{-\infty}^{\infty}\int_{-\infty}^{\infty}\int_{-\infty}^{\infty}\int_{-\infty}^{\infty} \mathfrak{F}\left(r_1,\, z_1,\, \vec{k},\, k_3,\, \omega\right) \mathfrak{F}^*\left(r_2,\, z_2,\, \vec{K},\, k_3,\, \nu\right) e^{ij\vec{k}\cdot\vec{H}_1} e^{-il\vec{K}\cdot\vec{H}_2}\, \langle\tilde{w}\tilde{w}^*\rangle\, d^2\vec{K}\, dK_3\, d^2\vec{k}\, dk_3 \tag{1}$$

Here, $\mathfrak{F}$ is the cascade response due to a unit upwash. $\mathfrak{F}$ was initially described in Appendix B of the report by Ventres[6] and extended via Graham's similiary rules for the present work to give the cascade response to a skewed gust (i.e. nonzero value of k_3).

When the upwash correlation is substituted into Eq. (1), one can complete the integration over $\vec{k}$ and k_3 using the delta functions. The RMS pressure on the vane which is required for comparison with the experimental data is obtained from the autocorrelation i.e. $r_1 = r_2$, $z_1 = z_2$, and $\omega = \nu$. Therefore

$$\langle \Delta p(r, z, \omega) \Delta p^*(r, z, \omega)\rangle = \frac{(\rho_o U_r u_b')^2}{(2\pi)} \int_{-\infty}^{\infty}\int_{-\infty}^{\infty}\int_{-\infty}^{\infty} \left|\mathfrak{F}\left(r,\, z,\, \vec{K},\, K_3,\, \omega\right)\right|^2 \delta(\omega - \vec{K}\cdot\vec{U_r})\Phi(\vec{K}, K_3) d\vec{K} dK_3 \tag{2}$$

where u_b' represents the average value of the turbulence intesity, and Φ the turbulence spectrum. The delta function can be used when the integration over K_1 is performed to obtain

$$\langle \Delta p(r, z, \omega) \Delta p^*(r, z, \omega)\rangle = \frac{(\rho_o U_r u_b')^2}{(2\pi)} \int_{-\infty}^{\infty}\int_{-\infty}^{\infty} \left|\mathfrak{F}\left(r,\, z,\, \frac{\omega - K_2 U_{r2}}{U_{r1}}, K_2,\, K_3\right)\right|^2 \Phi\left(\frac{\omega - K_2 U_{r2}}{U_{r1}}, K_2, K_3\right) dK_2 dK_3 \tag{3}$$

Thus, if Φ is selected as the Leipmann spectrum, and the vane response $\mathfrak{F}$ is known for the necessary ranges of K_2 and K_3 for a given frequency ω, then the integrations can be performed and the broadband response at that frequency obtained.

III. Experimental data

As part of the Source Diagnostic Test, vane surface measurements at multiple locations were taken. The placement of the experimental pressure ports is shown in Figure 1. The data were post processed at NASA. An example of the processed data from one pressure port on the low-count vane taken from the NASA report[5] is shown in Figure 2. The broadband feature at around 25kHz appears in most of the data. Its genesis is unknown and it will be shown that the current simulations do not predict such a feature.

Also shown in Figure 2 is the 1BPF content in the signal at each port. Comparison of the distribution of the pressure on the vane at the BPF and its harmonics makes sense and has been previously presented.[7] The broadband response does not lend itself to full vane distribution comparison at a specified set of frequencies. Instead, the broadband spectrum at various ports will be used for the comparisons in this paper.

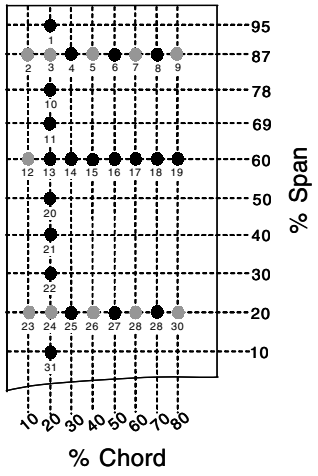

Figure 1. Pressure port locations on SDT low-count vane (Taken from NASA T M-2002-211809.[5])

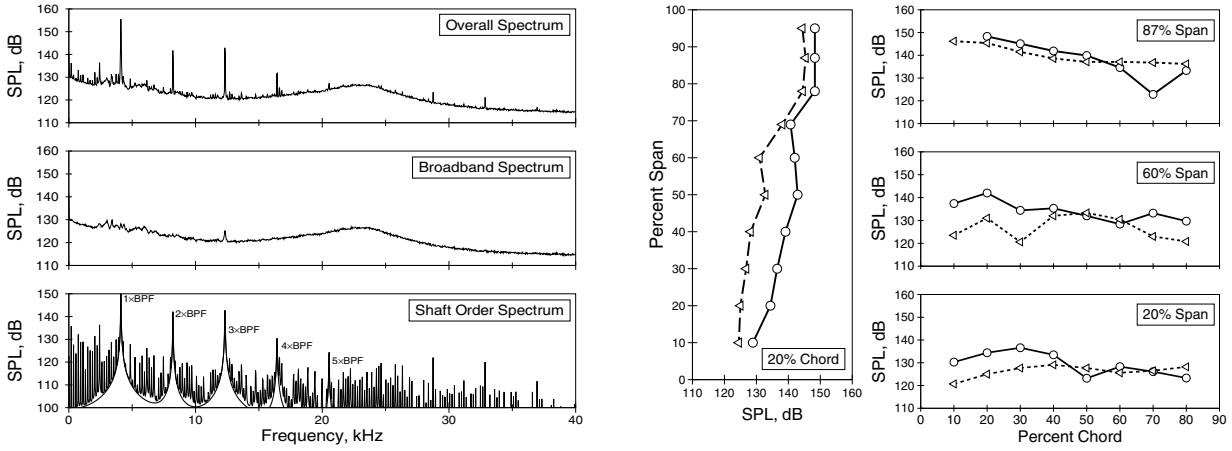

(a) Processed data at one port.

(b) Results for magnitude of BPF signal for ΔC_p (solid lines) and C_p at all ports.

Figure 2. Example Unsteady surface pressure data. Wide band analysis. (Taken from NASA T M-2002-211809.[5])

The experimental data taken from the SDT low-count vane configuration at the approach wheel speed from five ports along the 20% chord position are shown in Figure 3. These correspond to ports numbered 24, 20, 13, 10, and 1 in Figure 1. Figure 3 provides a plot of all of the data as well as a plot of the portion of the spectrum from 1 to 40 kHz. The truncated spectrum has been the focus of previous duct acoustic calculations and as such will be given attention in this paper. At the lowest frequencies a clear trend can be

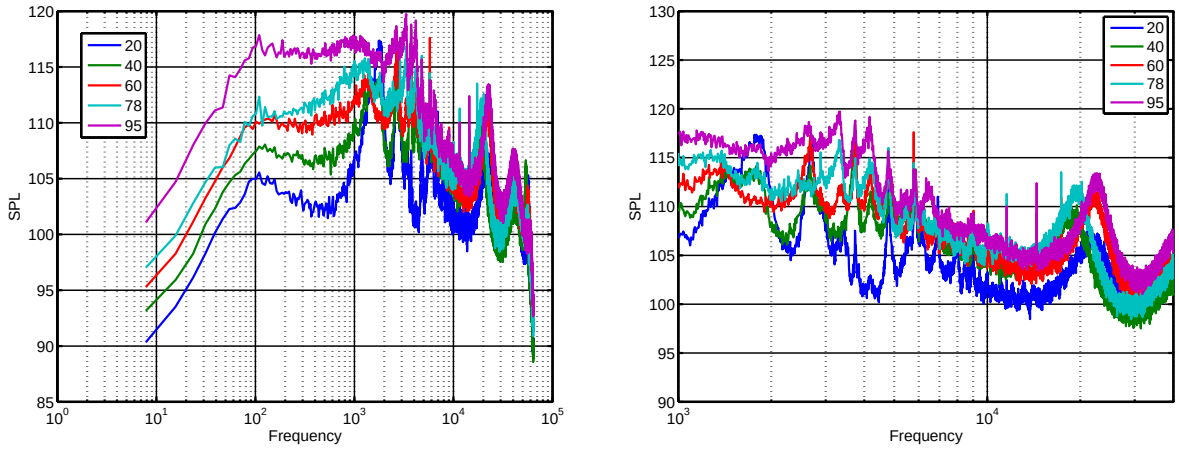

(a) All data. (b) Frequency range of interest.

Figure 3. Unsteady vane pressure at 5 spanwise locations along the 20 % chord.

seen with the lowest pressure at the hub and highest at the tip. At 10 kHz, the ordering is no longer clear.

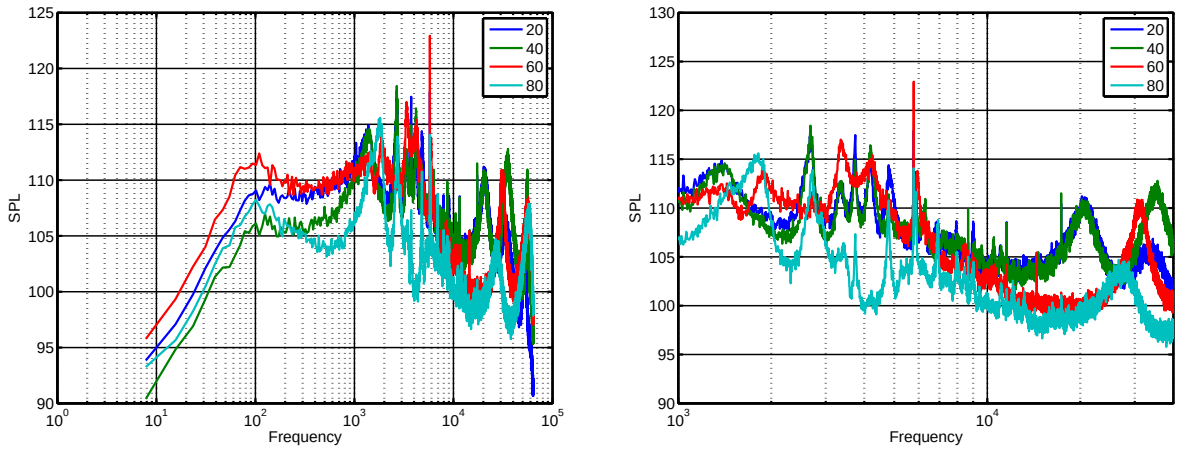

(a) All data. (b) Frequency range of interest.

Figure 4. Unsteady vane pressure at 4 chordwise locations along the 60 % span.

Similarly, the experimental data from four chord locations at the 60% span position are shown in Figure 4. As expected, the pressure tap at the 80% chord position measured the lowest RMS levels at most frequencies. Near 2 kHz the pattern deviates but the reason for the variation is unclear.

IV. Results

The broadband vane response for the SDT low-count vane at the approach condition was simulated using the RSI approach. A Leipmann spectrum was used to model the turbulence spectrum and only the average passage value of the turbulence intensity was used in the simulation. The wave number truncations for K_2 and K_3 were tested to ensure that the Fourier integrals in Eq. (3) had converged. The results for the RMS value of the pressure jump, Δp, are compared to the experimental data at nine of the pressure taps. The results at 20, 40 and 60 percent chord locations at 20, 60 and 87 percent span locations are shown in Figs. 5-6.

For the frequencies that have been plotted in Figs. 5-6, the prediction for frequencies above 10 kHz diverge from the experimental values with the predictions falling off much more rapidly than the experimental data. The trend from 1 kHz to 10 kHz is fairly well captured near the centerspan as seen in Figure 6(a), but at the hub and tip, the levels at the lower frequencies are underpredicted by the simulation.

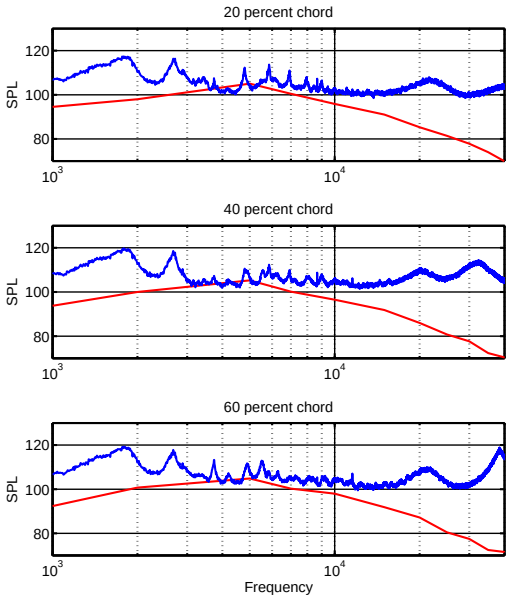

Figure 5. Computed vs measured RMS levels of pressure at 20% spanwise location.

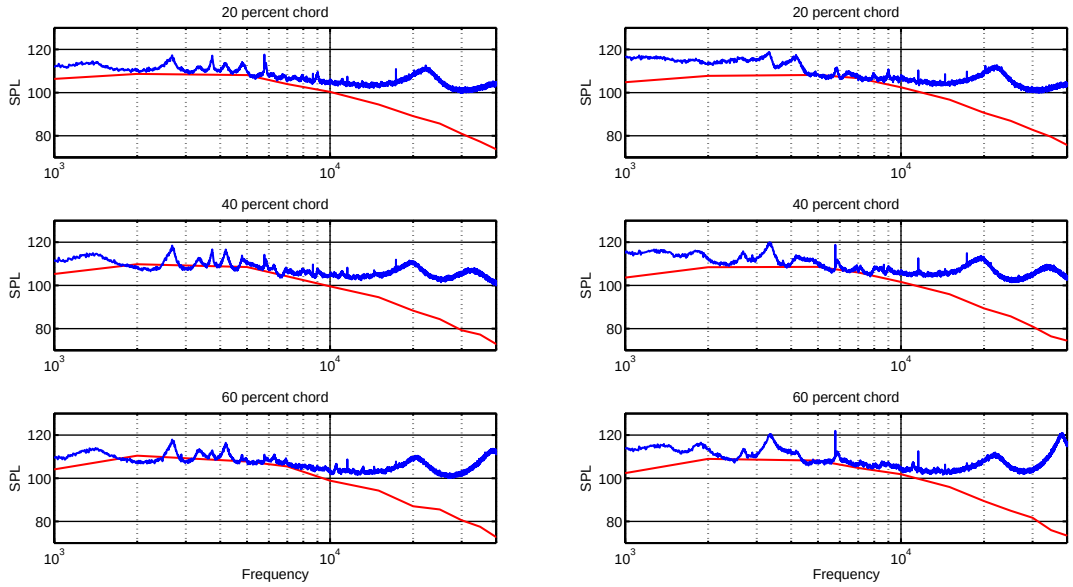

(a) 60 % span location.

(b) 87 % span location.

Figure 6. Computed vs measured RMS levels of pressure at 60% and 87% spanwise positions.

It is noted that the predicted vane response has a very similar character to the final exhaust duct power level shown in Figure 7. However, this means it is void of many of the features found in the experimental vane response data. Figure 7 shows the experimental acoustic spectra, the spectra predicted using RSI and the spectra predicted using two other methods.[2,3] They all predict the same spectral form and have a roll off above 10 kHz comparable to what is predicted for the vane pressure roll off. Therefore, if the vane response does not have this roll off, further explanation as to the link between the vane response and the final duct acoustics is required.

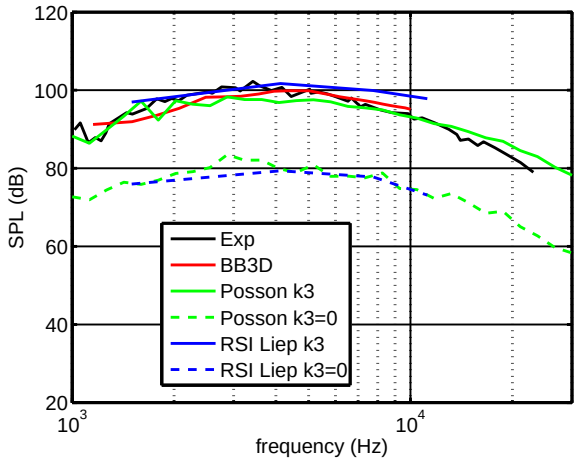

Figure 7. Broadband duct acoustic power level for lowcount SDT case, approach case. Computed using RSI, Posson's method without the annular correction, BB3D

In the near future it will be of interest to check the influence of two modeling parameters. First, the approach used by Posson et al[2] is very similar to the RSI method except that the formulation is derived in cylindrical coordinates from the start and incorporates an annular correction term in the rectilinear cascade response. At a single frequency, the annular correction leads to a difference in the vane response as shown in Figure 8. The influence on the broadband response when this effect is included must still be studied. Second, the RSI method can utilize a model for the inhomogeneity of the turbulence intensity in a passage. It was shown that when only the average passage value is used, the roll off above 10 kHz is increased.[4] Including the variation in the turbulence intensity may make the broadband vane response also roll off more slowly and thus be in better agreement with the data.

(a) Without annular correction

(b) With annular correction

Figure 8. Vane response strip theory method. With and without annular correction. Frequency: 5kHz; mode: 20; $k_3 = 1.5$ (normalized by half-chord), lowcount SDT case, approach case.

V. Conclusion

The broadband vane pressure response for the SDT low-count vanes at the approach condition has been simulated using the RSI method. The results have been compared to the experimental data. Investigation of solely the experimental data gives rise to questions regarding features present in the data above 20 kHz. Hopefully, future investigations will enable the understanding of these features. Between 1 and 20 kHz, the predicted broadband response matches well at 60% span, but at the hub and tip the RMS levels for frequencies under 4 kHz are underpredicted. Further rotor conditions must be simulated to help ascertain the root of these differences.

VI. Appendix

A. Upwash spectrum

The velocity fluctuations normal to the surface of the vanes can be assumed to have the following form.

$$w(\vec{X}, r, t) \approx w(\vec{X} - \vec{W}t, r) = F(\vec{X} \cdot \hat{n}, r) g(\vec{X} - \vec{W}t, r)$$

where $\vec{X} = (X_1, X_2)$, the "frozen gust" assumption is used to approximate the dependence on $\vec{X}$ and t independently by the linked argument $\vec{X} - \vec{W}t$. Here the vectors $\vec{X}$, $\vec{W}$, and $\hat{n}$ are taken to be in the moving rotor frame with $\vec{W}$ being the mean flow velocity and $\hat{n}$ being the unit normal to the stator vane. The correlation function of the upwash can be written as

$$\left\langle w(\vec{X} - \vec{W}t, r_1) w^*(\vec{Y} - \vec{W}\tau, r_2) \right\rangle \;=\; F(\vec{X} \cdot \hat{n}, r_1) F^*(\vec{Y} \cdot \hat{n}, r_2) R(\vec{X} - \vec{Y} + \vec{W}(t - \tau),\, \Delta r)\,, \qquad (4)$$

where

$$R(\vec{X} - \vec{Y} - \vec{W}(t - \tau),\, \Delta r) = \left\langle g(\vec{X} - \vec{W}t, r_1) g^*(\vec{Y} - \vec{W}\tau, r_2) \right\rangle$$

and $\Delta r = r_1 - r_2$. The function F describes the variation of RMS turbulence normal to the vane and R is a correlation function relating to the length scale of the turbulence. Both will be formally defined later in the derivation.

The desired result is the Fourier transform of the upwash correlation function with respect to both time and space in the stationary stator frame. Using the transform pair

$$s(x,t) = \frac{1}{4\pi^2} \int_{-\infty}^{\infty} \int_{-\infty}^{\infty} \hat{s}(\lambda) e^{-i\omega t + i\lambda x}\, d\lambda d\omega$$
$$\hat{s}(\lambda, \omega) = \int_{-\infty}^{\infty} \int_{-\infty}^{\infty} s(x) e^{i\omega t - i\lambda x}\, dx dt\,,$$

where s is an arbitrary function and $\hat{s}$ is its Fourier transform, we can write the desired result as follows.

$$\langle \tilde{w} \tilde{w}^* \rangle \;= \left\langle \tilde{w}(\vec{k}, k_3, \omega) \tilde{w}^*(\vec{K}, K_3, \nu) \right\rangle = \iint \iiint \iiint \; \langle w(\vec{x}, r_1, t) w^*(\vec{y}, r_2, \tau) \rangle \; e^{i\omega t - i\vec{k}\vec{x} - ik_3 r_1} e^{-i\nu\tau + i\vec{K}\vec{y} + iK_3 r_2}\, d\vec{x}\, dr_1\, d\vec{y}\, dr_2\, dt\, d\tau \qquad (5)$$

Here the integrals all range from $-\infty$ to ∞; ω and ν are radial frequencies; and, $\vec{k}$ and $\vec{K}$ are 2D wavenumber vectors. The third wave number has been separated in order to more easily track them in the derivation. The $\tilde{}$ indicates transform in two spatial dimensions and time.

Since the upwash velocity is most easily defined in the rotor frame (as above), rather than carry out the integration in the stator frame, we will use the following transformation to move all quantities to the rotor frame.

$$\begin{aligned} \vec{X} &= \vec{x} + \vec{D} + \Omega r_1 t \hat{e}_2 \\ \vec{Y} &= \vec{y} + \vec{D} + \Omega r_2 \tau \hat{e}_2 \end{aligned} \tag{6}$$

Thus, we can rewrite Eq. (5) as follows.

$$\begin{aligned} \langle \tilde{w}\tilde{w}^* \rangle \;=\; \iint \iiint \iiint \langle w(\vec{X} - \vec{W}t, r_1) w^*(\vec{Y} - \vec{W}\tau, r_2) \rangle \\ e^{i\omega t - i\vec{k}\cdot\left(\vec{X} - \vec{D} - \Omega r_1 t \hat{e}_2\right)} e^{-i\nu\tau + i\vec{K}\cdot\left(\vec{Y} - \vec{D} - \Omega r_2 \tau \hat{e}_2\right)} \; e^{-ik_3 r_1 + iK_3 r_2} d\vec{X}\, dr_1\, d\vec{Y}\, dr_2\, dt\, d\tau \end{aligned} \tag{7}$$

Next, substituting in Eq. (4) and using

$$\begin{aligned} \vec{\xi} = \vec{X} - \vec{Y} + \vec{W}(t - \tau) \Big\} \text{ Argument of } R \\ \xi_r = r_1 - r_2 \\ \Rightarrow \vec{X} = \xi + \vec{y} + \vec{W}(t - \tau) \Big\} \; \vec{X} \text{ in terms of } \vec{\xi} \text{ and } \vec{Y} \;, \end{aligned}$$

Eq. (7) can now be written in terms of $\vec{\xi}$, ξ_r and $\vec{Y}$, r_2.

$$\begin{aligned} \langle \tilde{w}\tilde{w}^* \rangle \;=\; \iint \iiint \iiint F((\vec{\xi} + \vec{Y}) \cdot \hat{n}, \xi_r + r_2) F^*(\vec{Y} \cdot \hat{n}, r_2) R(\vec{\xi}, \xi_r) \\ e^{i\omega t - i\vec{k}\cdot\left(\left(\vec{\xi} + \vec{Y} + \vec{W}(t-\tau)\right) - \vec{D} - \Omega r_1 t \hat{e}_2\right)} e^{-i\nu\tau + i\vec{K}\cdot\left(\vec{Y} - \vec{D} - \Omega r_2 \tau \hat{e}_2\right)} \\ e^{-ik_3(\xi_r + r_2) + iK_3 r_2} d\vec{\xi} d\xi_r\, d\vec{Y}\, dr_2\, dt\, d\tau \end{aligned} \tag{8}$$

The integrations with respect to t and τ are performed, resulting in

$$\begin{aligned} \langle \tilde{w}\tilde{w}^* \rangle \;=\; (2\pi)^2 \delta\left(\omega - \vec{k}\cdot\vec{W} + k_2\Omega r_1\right) \delta\left(\nu - \vec{K}\cdot\vec{W} + K_2\Omega r_2\right) \\ \iint \iiint \iiint F((\vec{\xi} + \vec{Y}) \cdot \hat{n}, \xi_r + r_2) F^*(\vec{Y} \cdot \hat{n}, r_2) R(\vec{\xi}, \xi_r) \\ e^{-i\vec{k}\cdot\vec{\xi}} e^{-i\vec{Y}\cdot(\vec{k} - \vec{K})} e^{i\vec{D}\cdot(\vec{k} - \vec{K})} e^{-ik_3(\xi_r + r_2) + iK_3 r_2} \; d\vec{\xi} d\xi_r\, d\vec{Y} dr_2 \;. \end{aligned} \tag{9}$$

A simplified form of the function F which describes the turbulence distribution across a passage is adopted now. The average passage value of the turbulence intensity is labeled u'_b so that

$$F(y) = u'_b \;.$$

Using this definition of F, the $F(\ldots)F^*(\ldots)$ term from Eq. (9) becomes simply

$$F\left((\vec{\xi} + \vec{Y}) \cdot \hat{n}\right) F^*\left(\vec{Y} \cdot \hat{n}\right) = \mathcal{F}_{bb} = \left(u'_b\right)^2 \tag{10}$$

Substituing Eq. (10) into Eq. (9) results in

$$\langle \tilde{w}\tilde{w}^* \rangle = (2\pi)^2 \delta\left(\omega - \vec{k}\cdot\vec{W} + k_2\Omega r_1\right) \delta\left(\nu - \vec{K}\cdot\vec{W} + K_2\Omega r_2\right) [\mathfrak{w}_{bb}] \tag{11}$$

where

$$\mathfrak{w}_{bb} = \iint \iiint \iiint \left(u'_b\right)^2 R(\vec{\xi}, \xi_r) e^{-i\vec{k}\cdot\vec{\xi}} e^{-i\vec{Y}\cdot(\vec{k} - \vec{K})} e^{i\vec{D}\cdot(\vec{k} - \vec{K})} \; e^{-ik_3(\xi_r + r_2) + iK_3 r_2} d\vec{\xi} d\xi_r \, d\vec{Y} dr_2 \tag{12}$$

The integration with respect to $\vec{Y}$ and r_2 can now be performed on Eq. (12).

$$\mathfrak{w}_{bb} = (2\pi)^3 \left(u_b'\right)^2 \delta\left(-(\vec{k}-\vec{K})\right) \delta\left(K_3 - k_3\right) e^{i\vec{D}\cdot(\vec{k}-\vec{K})} \iiint R(\vec{\xi},\, \xi_r) e^{-i\vec{k}\cdot\vec{\xi} - ik_3\xi_r}\, d\vec{\xi} d\xi_r \tag{13}$$

Now, note that in each case, the remaining integration is simply the Fourier transform of the function R. Therefore, we can write

$$\mathfrak{w}_{bb} = (2\pi)^3 \left(u_b'\right)^2 \delta\left(\vec{K}-\vec{k}\right) \delta\left(K_3 - k_3\right) e^{i\vec{D}\cdot(\vec{k}-\vec{K})} \Phi\left(\vec{k}, k_3\right) \quad . \tag{14}$$

Looking back at Eq. (11), we can now rewrite the arguments to its two delta functions. First, note that the term $-\vec{k}\cdot\vec{W} + k_2\Omega r_1$ from the first delta function in Eq. (11) can be simplified as follows

$$-\vec{k}\cdot\vec{W} + k_2\Omega r_1 = \vec{k}\cdot\left(-\vec{W} + \Omega r_1 \hat{e}_2\right) = -\vec{k}\cdot\vec{U}_{r_1}$$

Similarly

$$-\vec{K}\cdot\vec{W} + K_2\Omega r_2 = \vec{K}\cdot\left(-\vec{W} + \Omega r_2 \hat{e}_2\right) = -\vec{K}\cdot\vec{U}_{r_2}$$

Using these forms, the final correlation function of the upwash can be written as

$$\langle \tilde{w}\tilde{w}^* \rangle = (2\pi)^5 \left(u_b'\right)^2 \delta\left(\omega - \vec{k}\cdot\vec{U}_{r_1}\right) \delta\left(\nu - \vec{K}\cdot\vec{U}_{r_2}\right) \delta\left(\vec{K}-\vec{k}\right) \delta\left(K_3 - k_3\right) \Phi\left(\vec{k}, k_3\right) e^{i\vec{D}\cdot(\vec{k}-\vec{K})} \tag{15}$$

Acknowledgments

The authors would like to thank Dr. E. Envia of NASA Glenn for providing the relevant experimental test specifications and data and discussing the testing and related simulation work. The authors also acknowledge the financial support of the Aeroacoustics Research Consortium and collaboration of its members. Finally the authors thank Stephane Moreau and Jerome de Laborderie for supplying the results from the Posson method.

References

[1]Nallasamy, M. and Envia, E., "Computation of rotor wake turbulence noise," *Journal of Sound and Vibration*, Vol. 282, 2005, pp. 649–678.

[2]Posson, H., Moreau, S., and Roger, M., "Broadband noise prediction of fan outlet guide vane using a cascade response function," *Journal of Sound and Vibation*, Vol. 330, 2011, pp. 6153–6183.

[3]Atassi, H. M. and Logue, M. M., "MOdeling tonal and broadband interaction noise," *Procedia Engineering, IUTAM Symposium on Computational Aero-Acoustics for Aircraft Noise Prediction*, Vol. 6, 2010, pp. 214–223.

[4]Grace, S., Wixom, A., Winler, J., and Sondak, D. L., "Fan Broadband Interaction Noise Modeling," *AIAA Paper No. AIAA 2012-2269*, 2012, 18th AIAA/CEAS Aeroacoustics Conference.

[5]Envia, E., "Fan Noise Source Diagnostic Test-Vane Unsteady Pressure Results." *AIAA Paper No. 2002-2430*, 2002, 8th AIAA/CEAS Aeroacoustics Conference.

[6]Ventres, C., Theobald, M. A., and Mark, W. D., "Turbofan Noise Generation Volume 1: Analysis," Tech. Rep. CR-167952, NASA, July 1982.

[7]Sharma, A., Richards, S. K., Wood, T. H., and Shieh, C., "Numerical Prediction of Exhaust Fan Tone Noise from High Bypass Aircraft Engines," *AIAA Journal*, Vol. 47, No. 12, 2009.